JOURNAL OF SPACECRAFT AND ROCKETS
Vol. 36, No. 5, September–October 1999

Nanometer Regularity in the Mechanics of a Precision Deployable Spacecraft Structure Joint

Steven J. Bullock*
Hughes Space and Communications, Los Angeles, California 90009
and
Lee D. Peterson†
University of Colorado, Boulder, Colorado 80309-0429

The nonlinear microdynamics of a precision deployable space structure revolute joint incorporating angular contact ball bearings are investigated. Using a controlled-displacement force-state mapping method, it is shown that the hysteresis of the joint approaches material damping levels as the motions approach nanometer levels, both in extension and rotation. This suggests that structures developed from such a joint will be asymptotically linear at nanostrain motions. Moreover, the joint has regular microdynamics for displacements of nanometers and rotations of microradians. No mechanical irregularities are detected to at least 5 nm of extensional resolution and 20 nrad of rotational resolution. For extensions of 1 μm or less, the axial stiffness shows negligible hysteresis, which within the resolution of the test, is comparable to material damping. In rotation, the joint exhibits nonlinear rotational behavior consistent with Todd/Johnson hysteresis loops (Todd, M. J., and Johnson, K. L., "A Model for Coulomb Torque Hysteresis in Ball Bearings," *International Journal of Mechanical Science*, Vol. 29, 1987, pp. 339–354) and is repeatable down to torques of 10 μ-N-m. The data support the conclusion that machined irregularities in the bearing component surfaces result in smooth, rather than irregular, microdynamic response.

Nomenclature

b	= linear curve fit intercept
F_z	= axial force
$f(\dot{x}, x)$	= nonlinear restoring force
K_z	= extensional spring constant
K_θ	= hinge axis spring constant
M_θ	= hinge angle moment
m	= mass [Eq. (2)], linear slope [Eq. (4)]
s	= Dahl[4] model reversal slope
T	= rolling friction torque
T_s	= steady-state rolling friction torque
t	= time
u	= externally applied generalized force
x, y	= in-plane joint degrees of freedom
z	= axial joint degree of freedom
γ	= empirical Dahl[4] constant
θ	= joint rolling (hinge) angle
σ	= curve fit standard deviation
ϕ	= joint compliance angle (about x)
ψ	= joint torsion angle (about y)

Introduction

STRUCTURES are commonly deployed from spacecraft to form geometries larger than their respective launch vehicle shroud. In the past, only low-precision structures were deployed, such as communication antennas, solar arrays, and magnetometer booms. Recent developments in structures, mechanisms, and adaptive control technologies have lead to the consideration of very high-precision deployed structures for new science instruments, such as a large diameter optical telescope and a long baseline interferometer.

Before such instruments can be reliably engineered, it is important to understand the mechanics of high-precision deployed structures at very low levels of motions. Many future high-precision deployable instruments must be dimensionally stable to tens of nanometers. Although the mechanics of structural components are well characterized at macroscopic motion levels, little is available in the literature to describe the low-level mechanics that are critical to the engineering of high-precision deployable structures.

This paper presents results from low-level micromechanical testing of a new joint specifically developed for high-precision deployable structures. These results are the first extensive set of data to characterize the mechanical response of a revolute joint at these low levels of motion. In many previous precision deployable structures, the joints of were typically press fit and machined to high tolerances to achieve macroscopic shape stability.[1] Prior investigations, however, have never validated joint microdynamics at nanostrain levels.

The joint studied in this experimental investigation was designed to be microdynamically benign while retaining the characteristics of low deployment torque, large angular motion, and low cost (Fig. 1).[1] Specifically, the design of this angular-contact bearing joint eliminates most nonlinearities arising from joint freeplay and from friction. However, it was not known if the new design exhibits complex mechanical interactions at micrometer and nanometer levels of deformation. A particular concern was that contact surface tip asperities in the ball bearings and races might dominate the microdynamics, giving rise to a random nonlinear response. Electron microscope pictures show pits and grooves in a steel race (Fig. 2) and a steel ball bearing of the joint (Fig. 3) that have a typical size between 1 and 10 μm. These surface irregularities are the result of manufacturing processes and the material crystalline structure.

Furthermore, microdynamic testing of a precision deployable structure incorporating these joints has identified nonlinear response to dynamic loading of the same order of magnitude as the surface irregularities in the joints.[2] However, the Hertzian contact patch[3] between the ball bearing and race in these joints is approximately 60×280 μm, which implies that the effects of local irregularities (the tip asperities) within the contact patch may be smoothed by averaging over the contact patch. Thus, it is not known whether microdynamic instability in deployed structures are caused by mechanical irregularities in the joints or are an indirect result of smooth, nanoscopic microslip frictional interactions in the joints. The experiments described in this paper provide data on this issue as well.

Presented as Paper 96-1333 at the AIAA/ASME/ASCE/AHS/ASC 37th Structures, Structural Dynamics, and Materials Conference, Salt Lake City, UT, 15–17 April 1996; received 27 July 1998; revision received 14 January 1999; accepted for publication 16 January 1999.

*Technical Staff Engineer, Mail Stop D563, P.O. Box 92919, Structural Dynamics Department, Building S24; sjbullock@ccgate.hac.com. Member AIAA.

†Associate Professor, Center for Aerospace Structures, Department of Aerospace Engineering Sciences; Lee.Peterson@Colorado.edu. Senior Member AIAA.

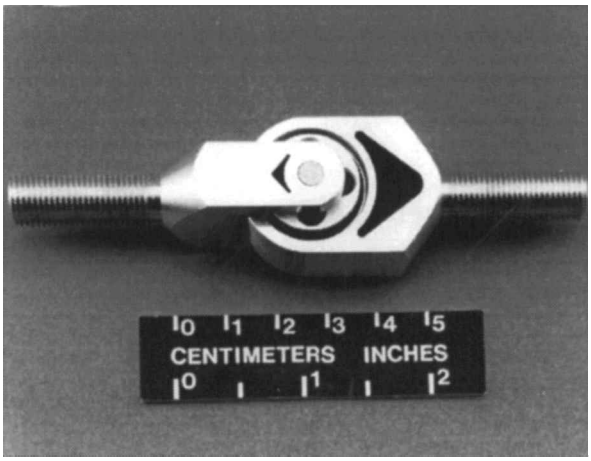

Fig. 1 NASA Langley Research Center precision deployable joint.

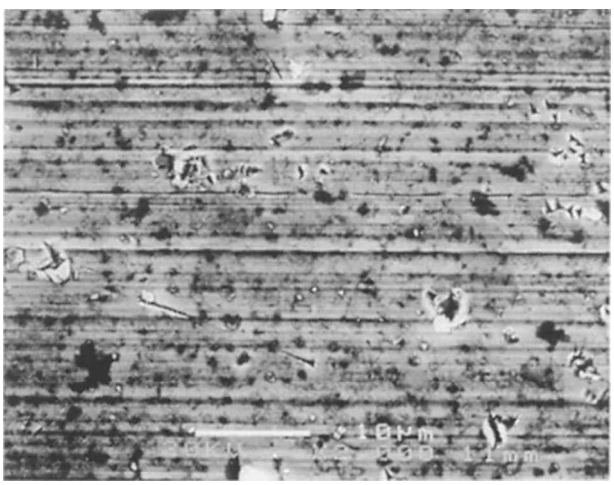

Fig. 2 Electron microscope photograph of the steel race surface at 10-μm scale.

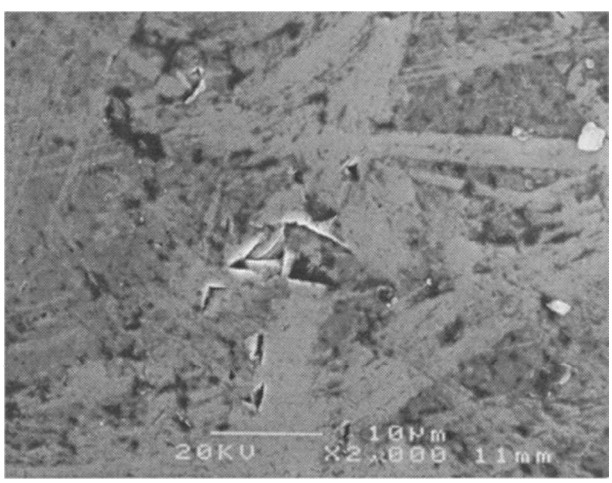

Fig. 3 Electron microscope photograph of the steel ball bearing surface at 10-μm scale.

If the Hertzian contact pressure dominates the friction characteristics, it is likely that an analytical model can be developed to describe the micromechanics of the joint. It has been experimentally observed that the friction torque of ball bearings at low rotational speeds (less than 1 deg/s) traces out hysteresis loops. Dahl[4,5] found a good fit to experimental data in the following model:

$$\frac{\mathrm{d}T}{\mathrm{d}\theta} = \gamma T_s^2 \left(1 - \frac{T \operatorname{sgn}\dot{\theta}}{T_s}\right)^2 \tag{1}$$

Many improvements and applications of the Dahl curve fit are reported by Todd and Johnson[6] and Lovell et al.[7,8] These previous studies were limited to rotations of hundreths of a radian or more. Downey et al.[9] demonstrated that an approximation of the Dahl curve fit explained ball bearing motions for oscillations of 25–1000 μrad at temperatures down to 4 K. (The actual motion was not measured.) Hachkowski and Peterson[10] experimentally measured steady rolling friction torques for the precision revolute joint consistent with predicted values,[6] but this work did not characterize the loops themselves. The Todd/Johnson model, in particular, is based on the critical assumption of contact mechanics: that friction behaves coulombically in a differential sense. This presumption might be expected to fail at microradians of rotation of a bearing when the proportion of slipped regions in a contact patch is small. It is, therefore, important to verify the Todd/Johnson model at such small rotations.

The primary objective of this paper is to draw conclusions about the micrometer- and nanometer-level microdynamics of the class of precision structural joints that would use ball bearings. More than the measurement of a particular joint design, comparison to predicted empirical results is used to extend the generality of the observations. Using a force-state map, the applicability of the Dahl curve fit for describing the joint's friction microbehavior is evaluated, as is the Todd/Johnson bearing model. These experiments will validate the Todd/Johnson theory at previously unmeasured levels of motion. As a result, the paper will draw conclusions about the effect of machine irregularities and about the variation of joint nonlinearity at nanostrain levels. Both conclusions will be important to the design of precision deployable structures, and neither can be found in the literature.

The remainder of this paper is organized as follows. In the first section, we review restoring force methods and the force-state mapping (FSM) technique. Next, the microbehavior FSM experiment is described in detail. A discussion of the axial and rotational test results follows. In the last section, the paper concludes with a summary of the joint's microbehavior.

Restoring Force Methods

In the results presented, the FSM method is used to measure nonlinear micrometer-level joint mechanics. The FSM technique is a subset of a class of nonlinear identification techniques, called restoring force methods, which has successfully experimentally identified nonlinear single degree of freedom (SDOF) and multiple degree of freedom and time-dependent systems.[11–19]

Restoring force methods assume that a physical, dynamic system obeys Newton's second law of motion for mass that is time invariant. For an SDOF system, the equation of motion is given by

$$m\ddot{x}(t) + f[\dot{x}(t), x(t)] = u(t) \tag{2}$$

The system mass can not be a direct function of time, but can be indirectly time dependent through dependence on the physical states. The function f is a general function of the internal or restoring force of the system. Therefore, if the acceleration and external force are measured, the restoring force can be determined by

$$f(\dot{x}, x) = u - m\ddot{x} \tag{3}$$

The measured restoring force can be visualized as a surface over the phase, or state, plane. This plot is called the force-state map of the system.

The restoring force method developed by Masri and Caughey[11] generated a model for f by fitting the measured data to a double expansion in Chebyshev polynomials in the variables $x(t)$ and $\dot{x}(t)$. Crawley and Aubert[12] used a general polynomial expansion to model f when they independently developed the FSM method. The usual procedure for determining the coefficients of either type of expansion is by a direct least-squares method. Studies[18,19] have shown that general polynomial expansions produce better results than Chebyshev expansions, which is the reason this work uses the FSM method.

The true strength of restoring force methods is their ability to fit experimental data to models of physical phenomena. Systems

with discontinuities in their stiffness or damping behavior,[14–16] hysteretic systems,[16] and systems with time-varying stiffness and damping properties[16] have all been experimentally identified. Restoring force methods can also accurately identify coulomb friction[14–16] and piecewise linear stiffness behavior.[16] When the behavior due to these physical phenomena is presented as a force-state map, a qualitative assessment of the influence of each type of phenomenon can be made due to the unique graphical features characteristic of each phenomenon.

Micrometer-Level FSM Experiment

Test Configurations

Figures 4 and 5 show the two test configurations used to measure the micrometer-level FSM. For the axial tests, an electrodynamic shaker attached to a backstop applied a force to the joint. A stinger from the shaker connected directly to a force transducer, that in turn was attached to the joint (Fig. 4). For the rotation tests, motion was induced using a piezoelectric translator (Fig. 5).

In both tests, the applied force was measured with an in-line force transducer. In the rotation tests, this force was resolved into the applied moment. The motion of the joint was measured by three noncontact fiber optic displacement gauges arranged to provide measurements of planar tilt, roll, and extension. The sensor target plate was not in the applied load path.

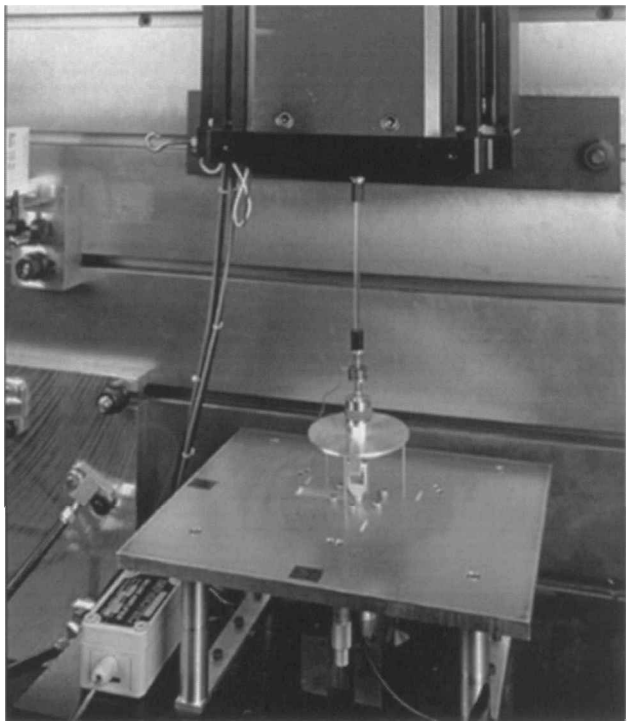

Fig. 4 Axial micro-FSM test configuration.

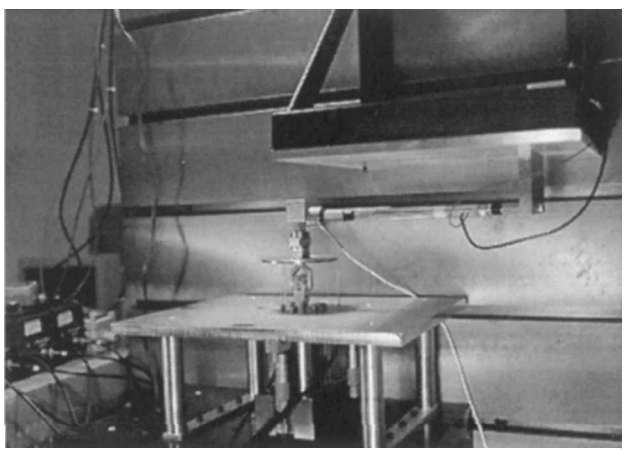

Fig. 5 Rotational micro-FSM test configuration.

The experiments are designed to determine the force-state map for the axial tension–compression state and for the rotation angle about the hinge line of an angular-contact bearing joint in its fully deployed configuration. Although the system inertia, damping, and stiffness tensors are dependent on the rotational state of the joint, they were always assumed to be tangentially constant because the testing procedure was carefully designed to keep the rotations on the order of microradians. Additionally, the excitation signals were chosen so that the inertia term was always less than 1% of the applied force or moment. The testing protocol made no attempt to counter gravity effects.

In developing and interpreting the results from an FSM experiment, it is important to consider two subtleties about the applied load and resulting motion. First, a force-state map is necessarily limited in range to a force-state region surrounding a nominal operating point of the experiment. In the experiments reported on in this paper, this operating point was around the 1-g weight of the test specimen. Any off-axis loads were mechanically regulated to be below the resolution of the test apparatus. Because the mass of the specimen was less than 1 N, the 1-g operating point offset was much less than the 20 N nominal applied loads. A more profound effect on the results is the use of a controlled-displacement actuation, rather than a controlled-load actuation. In a controlled-displacement actuation, the displacement is applied, and the resulting transmitted force is measured. In a controlled-load actuations, the load is applied, and the resulting displacement is measured. Although it is usual to use a controlled-displacement actuation in FSM methods, these results do not necessarily predict the response under a controlled-load actuation. In particular, this means that the experiments reported on here will characterize the microdynamic hysteresis of the joint, but not the microdynamic stability. Such experiments are the subject of future papers.

Data Collection Protocol

The equipment used to perform the experiment is diagrammed in Fig. 6. A master program communicates to all equipment through a parallel computer instrument interface and a multichannel input and output data acquisition board. A waveform generator program passes the waveform for a specific trial to the piezoactuator controller (or shaker power amplifier). The signal is then delivered to the piezoelectric actuator (or shaker). A data collection program loads previously defined experimental parameters. Next, the data collection program initializes the data acquisition board and the simultaneous track-and-hold module. Then the sensor gains and filter levels are set on a dc signal conditioner. The fiber optic sensors and the force transducer(s) send their signals to the dc signal conditioner during a test. The signals are amplified and filtered by an eighth-order Butterworth low-pass filter. A track-and-hold module simultaneously samples up to 8 channels, which are digitized by the 16-bit ADC on the data acquisition board. The filtered and digitized raw time data from each sensor are then recorded by the data collection program. A data analysis program performs additional data processing before generating FSM plots.

Experiment Parameters

The parameter choices for this study are shown in Tables 1 and 2 and are explained next. Data were collected at several different sampling rates between 80 and 800 Hz. The 80-Hz sample rate is slowest rate possible given the roll-off characteristics and minimum corner

Table 1 Experimental parameters

Parameters	Value
Sample rate	80–800 Hz
Sample points per channel	8,192, 16,384, or 32,768
Waveform for axial tests	10-Hz ramped sine wave
Waveform for rotation tests	0.025-, 0.1-, 0.5-, 1.0-, and 2.0-Hz sine waves
Axial force amplitude	20 N (~4.5 lbf)
Moment amplitudes	0.003–0.02 Nm (~0.4–3 in.-oz)

frequency (10 Hz) of the antialiasing filter. The higher sample rates are used to always provide at least nine full cycles of the excitation single while keeping the number of data points collected per channel to be 8192, 16,384, or 32,768. The high ratio of sample rate to excitation frequency provides very smooth, continuous displacement measurements. This high sample rate helps to minimize the errors introduced by differentiating the displacement measurements to obtain velocity and acceleration data. After no noticeable increase in numerical noise from differentiating signals with fewer sample points arose, most tests used 8192 sample points per channel to minimize data processing time.

The 10-Hz ramped sine wave for the axial tests produces the simplest excitation input signal that can adequately cover the state plane, i.e., all combinations of displacement and velocity. The five different sine waves for the rotation tests each use five different voltage amplitudes, which produce the moment amplitudes given in Table 1.

Analysis Protocol

Three general operations were performed on the scaled measurement data from each experiment. First the data were postprocessed in three phases. Phase 1 removed the average offset value in each ensemble of each sensor. This bias was removed because the fiber optic probes could only measure relative displacements, not absolute position. The second postprocessing phase filtered the data with a forward and backward second-order low-pass Butterworth filter with a corner frequency less than 10 Hz, iteratively determined to minimize both sensor noise and distortion of the signal. This step was required because the lowest antialiasing filter available in the hardware had a corner frequency of 10 Hz. The third phase removed any linear time drift from the signals by using a nonlinear least-squares algorithm with free variables for the dc offset, slope of the linear time drift, and amplitude, frequency, and phase angle of the sine wave. The linear time drift observed in the displacement gauges was most likely due to thermal drift within the laboratory environment.

The six rigid-body DOFs of the joint are 1) the axial translation motion due to tension and compression, z, 2) the translational motion that parallels the hinge line of the joint, y, 3) the translational motion perpendicular to the other two, x, 4) the compliance angle rotation ϕ, 5) the hinge angle rotation θ, and 6) the torsion angle rotation ψ. Of the six rigid-body DOFs and six generalized applied forces, only the z, ϕ, and θ states and the F_z and M_θ forces were observable due to the number and placement of sensors and the force transducers.

The primary assumption of all of the equations used in this stage of the analysis is that the joint, test fixtures, and target plate (see Fig. 4) remain rigid under all of the applied loads. This assumption implies that the kinematics of the test apparatus need include only the six rigid-DOFs of the joint. With this known geometry information and the rigid-body kinematic equations of motion, the three observable states can be determined from the three displacement measurements if the unobservable states are assumed to be zero. A Newton–Raphson procedure[20] extracted the observable states from the sensor measurements in this manner.

The third data operation differentiated the displacement measurements of the extracted states to obtain velocity and acceleration estimates by a five-point central difference rule. With the estimated axial and rotational state measurements, a program utilizing the Levenberg–Marquardt nonlinear least-squares method[20] identified nonlinear parametric models of the joint's microbehavior. This process is described in the results sections.

Validation Tests

An experiment to validate the testing and analysis protocols was performed on an aluminum rod. The rod had a 9.5-mm diam and a length of 6.2 cm. Tests of the rod in both axial and rotational configurations provided a measurement of the stiffness of the test apparatus, which was found to be approximately 10 times stiffer than the axial stiffness of the joint. The test apparatus was also found to have no resonances below 40 Hz. This experiment validated the key assumption of the data analysis protocol: that the dynamic behavior of both the test article and test apparatus could be ignored and that only rigid-body motions and static displacements are induced in the test specimen.

Table 2 Identified values of T_s and s from all amplitudes

Excitation frequency, Hz	T_s, Nm		s, Nm/rad		σ_{fit}, %	
	Mean	σ	Mean	σ	Mean	σ
0.025	0.134	0.088	132	8.0	0.34	0.20
0.100	0.103	0.032	136	8.1	0.33	0.18
0.500	0.129	0.048	140.	7.1	0.32	0.20
1.000	0.118	0.044	138	7.9	0.29	0.18
2.000	0.124	0.045	138	6.6	0.23	0.12

Axial Test Results

Figure 7 shows a scatter plot of 8192 data points from a 10-Hz ramped sine wave test presented as a force-displacement plot. Figure 8 presents the corresponding force-state map. The measured displacements and forces, after filtering, have a resolution of 5 nm and 0.01 N, respectively. It should be noted that these results do not identify the joint's stiffness alone, but also include the effects of the axial stiffness of the test apparatus. The mean effective stiffness of the joint embedded in the test apparatus is 20.5×10^6 N/m with a standard deviation of 5.31×10^4 N/m over 30 ensembles (less than

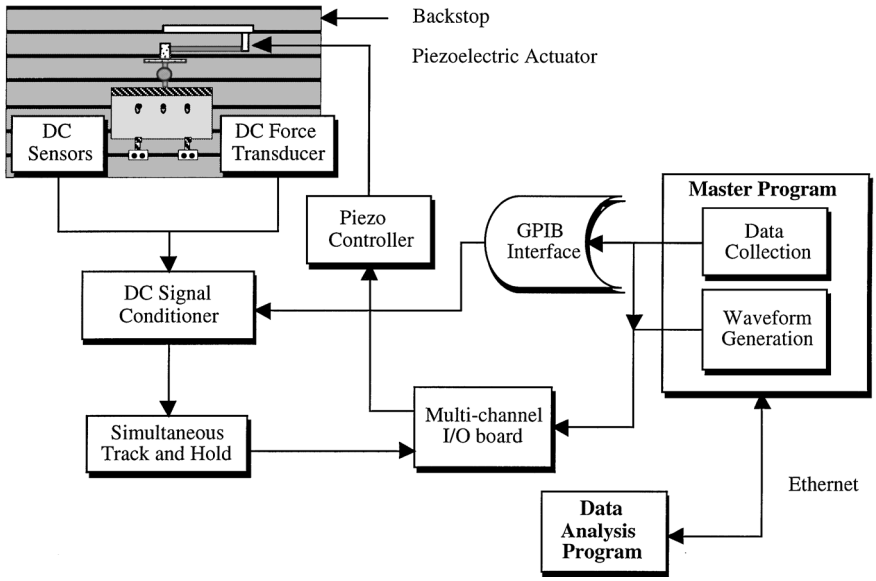

Fig. 6 Data acquisition system block diagram.

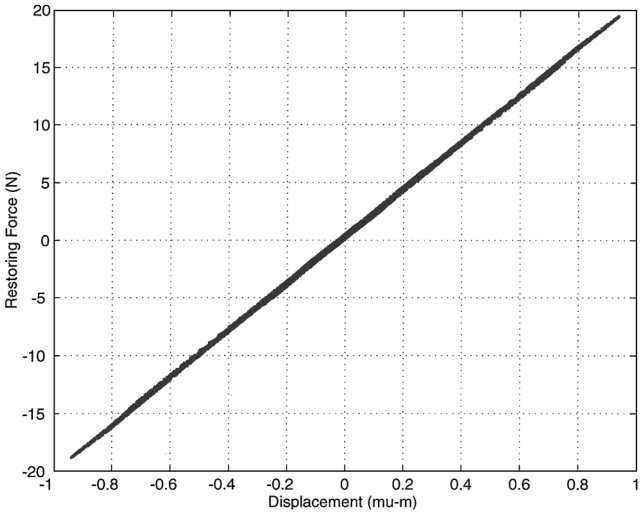

Fig. 7 Axial force-displacement behavior of the joint.

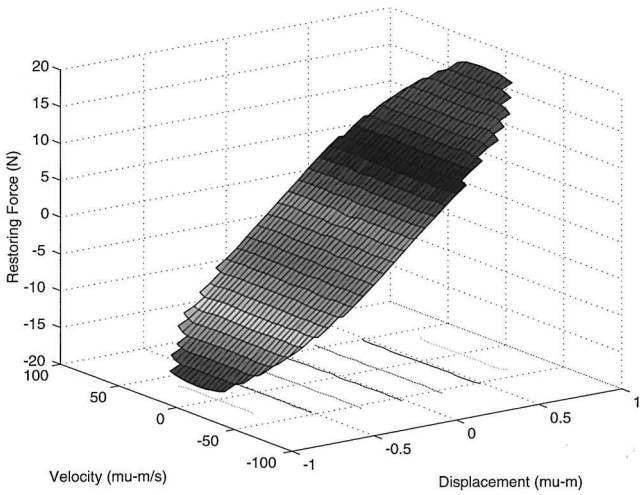

Fig. 8 Force-state map for the axial state.

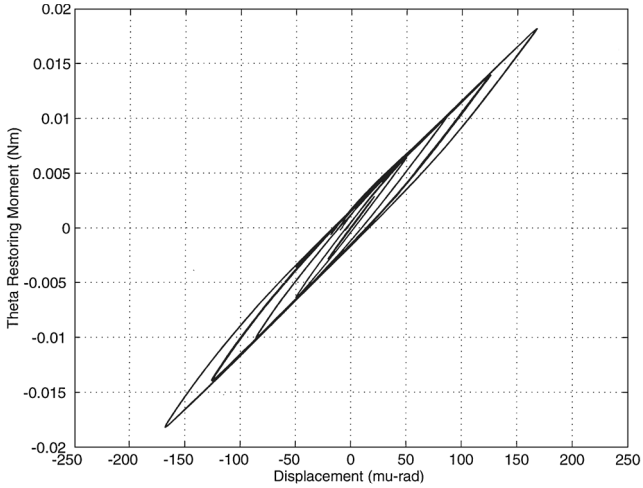

Fig. 9 Torque-rotation behavior (0.5-Hz sine wave excitation).

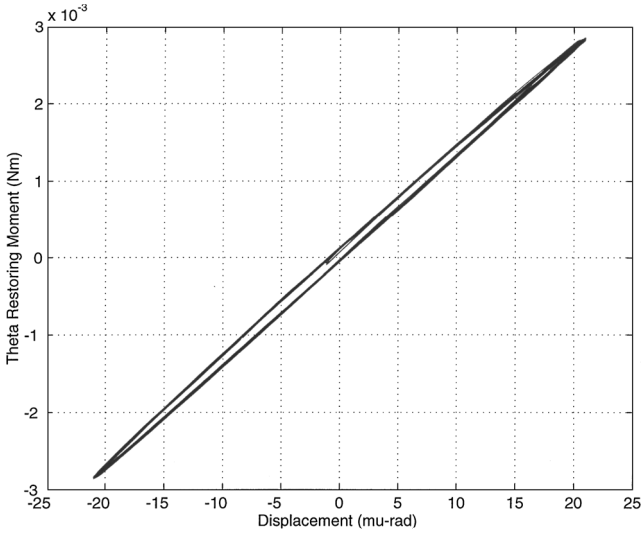

Fig. 10 Fine detail of the 0.5-Hz sine wave excitation experiment.

0.3%). As discussed extensively in Ref. 21, the small amount of hysteresis was too small to distringush between linear viscous damping, coulombic friction, or structural-type damping model forms. All three models provide very high agreement with the data but result in comparably uncertain estimates of the low identified loss factors. However, the estimates of the loss factors were all of the order of 0.5–1.5%, which is consistent with the material hysteresis in the ball bearing components themselves.

Thus, although the precise form of the hysteresis cannot be determined, it can be stated that nanostrain extensions in this particular joint result in negligible nonlinearity due to friction.[21] This behavior is markedly different from typical pin-clevis joints. Down to the submicrometer level, the axial behavior in this joint is linear. The lack of a velocity-dependent step in the FSM indicates that coulomb sliding friction is also absent from the angular-contact bearing joint in extension. This implies that all of the loss factor observed in this low-level test could be attributed to material hysteresis or to microslip friction with comparable certainty. In other words, in extension, this joint is indistinguishable from monolithic materials at nanostrain levels.

Rotational Test Results

Submicrometer Regularity in Rotation

Hypothesizing that the tip asperities on the ball bearings and races would only interact when the joint rotates, it was thought that more nonlinear behavior might be observed in the rotation tests than in the extension tests. To get the displacement control necessary to rotate the joint through microradians, a piezoactuator (Fig. 5) replaced the shaker of the axial tests.

Instead of ramping a sine wave up and down to sweep out the state plane, the excitation signals for the rotation tests were sine waves with five discrete amplitudes. This change allowed the experimental results to be used to identify nonlinear behavior while facilitating the comparison of the measured rotational motion to that predicted by the Todd/Johnson model of bearing friction.

Figure 9 shows the observed behavior at all five discrete excitation amplitudes for the 0.5-Hz sine wave excitations. Each hysteresis loop consists of eight complete cycles of three separate ensembles. Each separate ensemble is individually centered about the origin. Figure 10 magnifies the innermost set of hysteresis curves for the 0.5-Hz sine wave excitations.

The first conclusion of these tests is that the precision joint's rotational microbehavior is measurably nonlinear. However, the response is repeatable and predictable within the measurement resolutions, which were 20 nrad (4 m-arcseconds) of rotation and 1.2×10^{-5} Nm of applied moment. Although nonlinear, the rotational microbehavior is not complex nor does it exhibit the irregularity one might have expected from the contact patch tip asperities.

Dahl Hysteresis Curve Fits

The data suggest that the Hertzian contact patch mechanics govern friction behavior in this regime of motion and that, therefore, the data might be consistent with Dahl[4,5] hysteresis loops observed at macroscopic rotations. The microradian rotation data in fact display several characteristics of these loops. First, the joint experiences positive angular velocities while moving along the upper branch of the hysteresis curve and, similarly, negative angular velocities along the bottom branch. Second, the hysteresis loops are nested inside

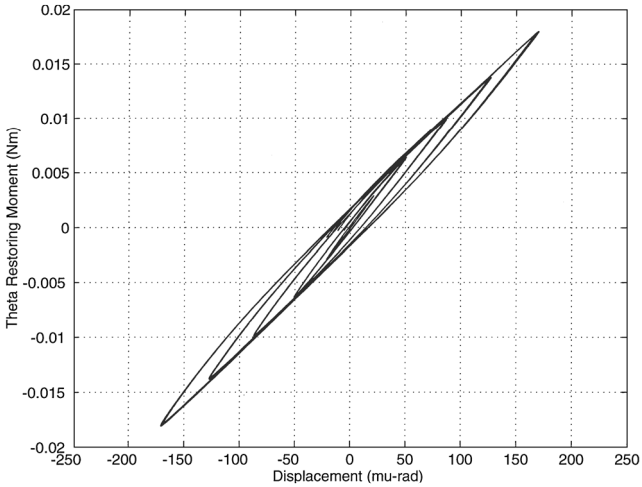

Fig. 11 Torque-rotation behavior (1.0-Hz sine wave excitation).

other hysteresis loops as the amplitude of angular displacement is increased. The third important characteristic of Dahl hysteresis loops is that the steady rolling friction torque is independent of the magnitude of the joint's angular velocity about the bearing axis for low speeds (less than 1 deg/s).

To verify this, the joint's peak angular velocities were varied by changing the frequency of the excitation sine wave. Figure 11 shows the rotational microbehavior for the joint under 1.0-Hz sine wave excitations. Like the 0.5-Hz data plotted in Fig. 10, each thick hysteresis curve is the result of plotting 24 cycles from three distinct ensembles. Comparison with Fig. 10 verifies the invariance of the hysteresis curves with changes in velocity.

Verification of the Todd/Johnson Model

Todd and Johnson derived an analytical model that can predict the shape of the Dahl hysteresis curves and the magnitude of the steady rolling friction torque to within 10–20% of the theoretical value.[6] Their model assumes that the shape of the curves is independent of the magnitude of the angular velocity about the bearing axis. Furthermore, they presume that the reversal slope s is independent of amplitude, but that otherwise the bearing friction hysteresis curve is determined by the Dahl empiricism. We note that the independence of the reversal slope s on amplitude is required by elasticity and contact mechanics, but is generally not guaranteed by the Dahl empiricism. The success of identifying both the steady rolling friction torque T_s and the reversal slope s from the experimental data will validate the Todd/Johnson model at microradians of rotation.

A nonlinear least-squares curve-fit algorithm extracted an estimate of the friction torque and slope from each branch of the 24 hysteresis loops measured at a given excitation amplitude. The standard deviation in the estimates of the friction torque and slope were 1.2×10^{-4} Nm and 0.022 Nm/rad, respectively. The identified values for all of the experiments, over all excitation levels, are presented in Table 2. In general, the model-fit error from all excitation frequencies is 0.3%, and the standard deviations imply that over 99% of the responses would have a model-fit error less than 1%. Thus, to within the accuracy of the day-to-day experimental repeatability, the joint's microbehavior is accurately described by Dahl hysteresis loops.

The next question is whether the Todd/Johnson model can predict the observed behavior. As reported in Ref. 10, the analytical prediction of the steady rolling friction torque for this precision joint is 3.5×10^{-3} Nm, and the experimentally measured value is 3.2×10^{-3} Nm. The experimentally identified friction torque values, presented in Table 2, are about 40 times higher than either of these values. Several systematic uncertainties in the test apparatus may explain this higher observed friction. The most likely cause is the flexure connected to the piezoactuator, which applies a restoring moment as the joint is rotated (see Fig. 5). The flexure, assumed to behave as a linear torsion spring, distorts the hysteresis curves into the observed shape, effectively masking the true hysteretic behavior. The next section discusses an experiment used to estimate the magnitude of this systematic error.

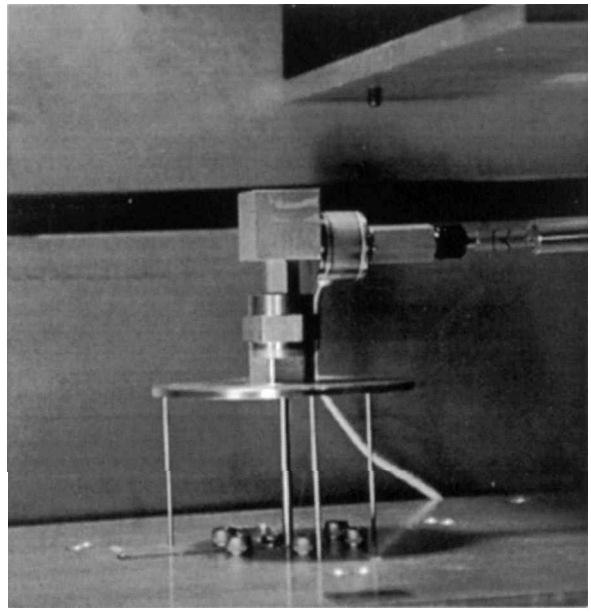

Fig. 12 Steel calibration test specimen used to identify parasitic rotational stiffness in the apparatus.

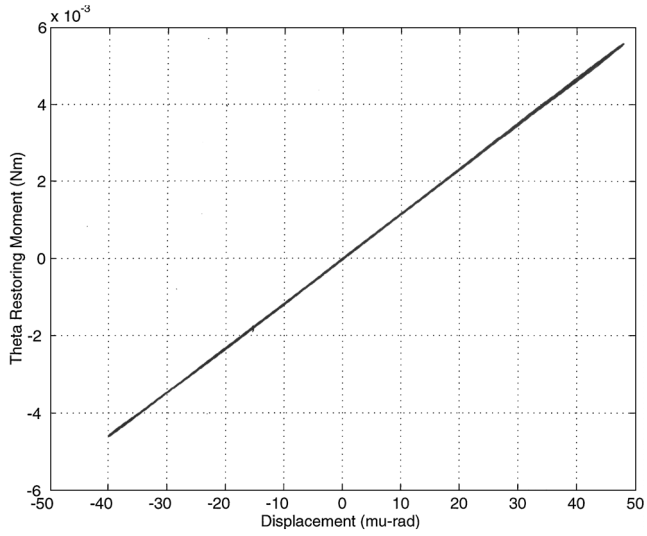

Fig. 13 Torque-rotation behavior of the steel calibration test specimen.

Steel Calibration Beam Tests

A simple experiment using a steel calibration beam was performed to identify the flexure's torsional stiffness. The beam had a diameter of 3.71 mm and a length of 54.5 mm (Fig. 12). Five tests recorded the axial displacement and angular rotation of the beam's tip under comparable displacements used in the beam tests. The first set of three tests excited the beam with the flexure rotated about 30 deg from the vertical. The second set of two tests recorded the beam's tip response with the flexure oriented vertically.

The rotation experienced by the steel beam's tip with changing restoring moment is shown in Fig. 13. Figure 13 shows the beam's responses to eight cycles of 0.5-Hz sine wave excitation. An important conclusion is reached after comparing the beam's tip rotations with the joint's microbehavior in Fig. 10: the observed behavior ascribed to the joint does in fact come from the joint and not the test apparatus. Through comparison of the two sets of calibration beam tests, it was proved that the beam's (or joint's) microbehavior is independent of the flexure's orientation.

The extremely linear microbehavior promised to clearly identify the parasitic torsional stiffness of the test apparatus that was assumed to be concentrated in the flexure. Two analytical models were derived to perform the nonlinear least-squares curve fit to the data. The first model assumed that all parasitic torsional stiffness could be lumped into a torsional spring attached to the tip of the beam. The second model added a linear spring, connected to ground, at the end of a rigid offset that was attached to the beam's tip. This spring provided a moment arm for this nonphysical linear spring to couple into the beam's tip rotation behavior.

The identified torsional spring constant for the first model, over all 15 ensembles, is 139.6 Nm/rad with a standard deviation of 1.1 Nm/rad. The second model produced a family of solutions for the identified hinge spring constant K_θ and linear spring constant K_x, which satisfied the following relationship:

$$K_x = mK_\theta + b \tag{4}$$

Over all 15 ensembles, the identified value of m is -140 rad/m^2 with a standard deviation of 1 rad/m^2. Similarly, b has a value of 18,600 N/m with a standard deviation of 10 N/m. When taken with the physically realizable values for K_θ, Eq. (4) gave equivalent torsional spring constants from 100 to 116 Nm/rad. Therefore, the uncertainty in the equivalent torsion spring constant varies significantly just from the choice of model. In contrast, the observed joint rotation behavior would agree with the predictions of the Todd/Johnson model if the identified equivalent torsional spring constant were approximately 57 Nm/rad. This implies that neither model for the parasitic stiffness in the test apparatus could account for the higher levels of hysteresis observed in rotation.

Conclusions

The experimental identification of the nonlinear microdynamics for an angular-contact bearing joint was reported. The FSM method was used to identify the behavior of the joint under very low applied moments and rotations of microradians. No mechanical irregularities were detected to at least 5 nm of extensional resolution and 20 nrad of rotational resolution. This implies surface irregularities in the bearing contact surfaces do not result in irregularity in the joint's low-level mechanics, which means that the joint micromechanics are determined by the averaging effect of the Hertzian contact patch rather than the machined irregularities in the bearing component surfaces.

Perhaps the most significant observation was that the nonlinearity, both in extension and in rotation, collapses to material hysteresis levels for microscopic motions and rotations. In extension, submicrometer strains resulted in an amount of hysteresis so small that it could not be distinguished from material damping in the joint. For microradians of rotation, the hysteretic loss factor was also significantly reduced (as predicted by the Dahl empirical model). Both of these facts suggest that it may be possible for precision deployable structures constructed from this type of joint to behave asyptotically as linear as the materials themselves in the low-level (submicrometer) range of motion.

Finally, the Todd/Johnson physical model of bearing friction agreed with the data somewhat. In particular, the independence of reversal slope with amplitude was successfully verified at nanoscopic motion amplitudes. However, very small residual stiffnesses in the apparatus did not allow quantitative verification of the Todd/Johnson friction values.

Acknowledgments

This work was supported by the Center for Space Construction through NASA Training Grant NTG-10033, by NASA Langley Research Center through NASA Grant NAG-1-1490, by NASA Training Grant NTG-10033 under the University Space Engineering Research Center Fellowship Program, by the NASA In-Space Technology Experiments Program through Contract NASW-4873, and by NASA Langley Research Center through Grants NAG1-1700 and NAG1-1840.

References

[1]Lake, M. S., Warren, P. A., and Peterson, L. D., "A Revolute Joint with Linear Load-Displacement Response for Precision AIAA-Deployable Structures," *Proceedings of the AIAA/ASME/ASCE/AHS/ASC 37th Structures, Structural Dynamics, and Materials Conference*, AIAA, Reston, VA, 1996, pp. 1639–1647.

[2]Warren, P. A., and Peterson, L. D., "Nonlinear Post-Deployment Micro-Mechanics of Precision Deployable Space Structures," *Proceedings of the AIAA/ASME/ASCE/AHS/ASC 37th Structures, Structural Dynamics, and Materials Conference*, AIAA, Reston, VA, 1996, pp. 2364–2373.

[3]Timoshenko, S., and Goodier, J. N., *Theory of Elasticity*, 3rd ed., McGraw–Hill, New York, 1951, pp. 409–420.

[4]Dahl, P. R., "A Solid Friction Model," Aerospace Corp., TOR-158(3107-18), Los Angeles, CA, May 1968.

[5]Dahl, P. R., "Solid Friction Damping in Mechanical Vibrations," *AIAA Journal*, Vol. 14, No. 12, 1976, pp. 1675–1682.

[6]Todd, M. J., and Johnson, K. L., "A Model for Coulomb Torque Hysteresis in Ball Bearings," *International Journal of Mechanical Science*, Vol. 29, 1987, pp. 339–354.

[7]Lovell, M. R., Khonsari, M. M., and Marangoni, R. D., "Low-Speed Friction Torque on Balls Undergoing Rolling Motion," *Tribology Transactions*, Vol. 36, No. 2, 1993, pp. 290–296.

[8]Lovell, M. R., Khonsari, M. M., and Marangoni, R. D., "Experimental Measurements of the Rest-Slope of Steady Torque on Ball Bearings Experiencing Small Angular Rotations," *Tribology Transactions*, Vol. 37, No. 2, 1994, pp. 261–268.

[9]Downey, C. H., Houck, J. R., Kubitschek, M. J., and Tarde, R. W., "Arcsecond Grating Drive Mechanism for Operation at 4 K," *Cryogenics*, Vol. 31, Dec. 1991, pp. 1030–1037.

[10]Hachkowski, M. R., Peterson, L.D., and Lake, M. S., "Friction Model of a Revolute Joint for a Precision Deployable Spacecraft Structure," *Journal of Spacecraft and Rockets*, Vol. 36, No. 4, 1999, pp. 591–598.

[11]Masri, S. F., and Caughey, T. K., "A Nonparametric Identification Technique for Nonlinear Dynamic Problems," *Journal of Applied Mechanics*, Vol. 46, 1979, pp. 433–447.

[12]Crawley, E. F., and Aubert, A. C., "Identification of Nonlinear Structural Elements by Force-State Mapping." *AIAA Journal*, Vol. 24, No. 1, 1986, pp. 155–162.

[13]Masri, S. F., Sassi, H., and Caughey, T. K., "Nonparametric Identification of Nearly Arbitrary Nonlinear Systems," *Journal of Applied Mechanics*, Vol. 49, 1982, pp. 619–627.

[14]Aubert, A. C., Crawley, E. F., and O'Donnell, K. J., "Measurement of the Dynamic Properties of Joints in Flexible Space Structures," M.S. Thesis, Dept. of Aeronautics and Astronautics, Massachusetts Inst. of Technology, Cambridge, MA, Sept. 1983.

[15]Masters, B. P., and Crawley, E. F., "Multiple Degree of Freedom Force-State Component Identification," *Proceedings of the AIAA/ASME/ASCE/AHS/ASC 34th Structures, Structural Dynamics, and Materials Conference*, AIAA, Washington, DC, 1993, pp. 3071–3085.

[16]Worden, K., "Parametric and Nonparametric Identification of Nonlinearity in Structural Dynamics," Ph.D. Dissertation, Heriot–Watt Univ., Edinburgh, Scotland, UK, Nov. 1989.

[17]Worden, K., and Tomlinson, G. R., "Parametric and Nonparametric Identification of Automotive Shock Absorbers," *Proceedings of the 10th International Modal Analysis Conference*, San Diego, CA, 1992, pp. 764–771.

[18]Al-Hadid, M. A., and Wright, J. R., "Developments in the Force-State Mapping Technique for Non-Linear Systems and the Extension to the Location of Non-Linear Elements in a Lumped-Parameter System," *Journal of Mechanical Systems and Signal Processing*, Vol. 3, 1989, pp. 269–290.

[19]Al-Hadid, M. A., and Wright, J. R., "Application of the Force-State Mapping to the Identification of Nonlinear Systems," European Forum on Aeroelasticity and Structural Dynamics, Aachen, Germany, 1989.

[20]Press, W. H., Teukolsky, S. A., Vetterling, W. T., and Flannery, B. P., *Numerical Recipes in FORTRAN*, Cambridge Univ. Press, New York, 1986, pp. 521–528.

[21]Bullock, S.J., "Identification of the Nonlinear Micron-Level Mechanics of Joints for Deployable Precision Space Structures," Ph.D. Dissertation, Dept. of Aerospace Sciences, Univ. of Colorado, Boulder, CO, May 1996.

R. B. Malla
Associate Editor